



A model incorporating clinicopathologic and liver imaging reporting and data system-based magnetic resonance imaging features to identify hepatocellular carcinoma in LR-M observations

Xin-Xing Hu* 
Dong Bai* 
Zhen-Lei Wang 
Yi Zhang 
Jue Zhao 
Mei-Ling Li 
Jia Yang 
Lei Zhang 

*Contributed equally to this work as the first authors.

From the Department of Radiology (X-X.H., Y.Z., J.Z., M-L.L., J.Y., L.Z. ✉ lei.zhang2@shgh.cn), Shanghai General Hospital, Shanghai Jiao Tong University School of Medicine, Shanghai, China; Department of Anesthesiology (D.B.), Shanghai Municipal Hospital of Traditional Chinese Medicine, Shanghai University of Traditional Chinese Medicine, Shanghai, China; Department of General Practice (Z-L.W.), Changhai Hospital, Naval Military Medical University, Shanghai, China.

Received 25 May 2023; revision requested 28 June 2023; accepted 11 August 2023.



Epub: 04.09.2023

Publication date: 07.11.2023

DOI: 10.4274/dir.2023.232215

PURPOSE

To evaluate the predictive value of a combination model of Liver Imaging Reporting and Data System (LI-RADS)-based magnetic resonance imaging (MRI) and clinicopathologic features to identify atypical hepatocellular carcinoma (HCC) in LI-RADS category M (LR-M) observations.

METHODS

A total of 105 patients with HCC based on surgery or biopsy who underwent preoperative MRI were retrospectively reviewed in the training group from hospital-1 between December 2016 and November 2020. The LI-RADS-based MRI features and clinicopathologic data were compared between LR-M HCC and non-HCC groups. Univariate and least absolute shrinkage and selection operator regression analyses were used to select the features. Binary logistic regression analysis was then conducted to estimate potential predictors of atypical HCC. A predictive nomogram was established based on the combination of MRI and clinicopathologic features and further validated using an independent external set of data from hospital-2.

RESULTS

Of 113 observations from 105 patients (mean age, 61 years; 77 men) in the training set, 47 (41.59%) were classified as LR-M HCC. Following multivariate analysis, aspartate aminotransferase >40 U/L [odds ratio (OR): 4.65], alpha-fetoprotein >20 ng/mL (OR: 13.04), surface retraction (OR: 0.16), enhancing capsule (OR: 5.24), blood products in mass (OR: 8.2), and iso/hypoenhancement on delayed phase (OR: 10.26) were found to be independently correlated with LR-M HCC. The corresponding area under the curve for a combined model-based nomogram was 0.95 in the training patients (n = 113) and 0.90 in the validation cohort (n = 53).

CONCLUSION

The combined model incorporating clinicopathologic and MRI features demonstrated a satisfactory prediction result for LR-M HCC.

KEYWORDS

Liver Imaging Reporting and Data System, hepatocellular carcinoma, LR-M, magnetic resonance imaging, model

The Liver Imaging Reporting and Data System (LI-RADS) is a comprehensive, dynamic system that is constantly updated with user feedback, evolving knowledge, and technological advancements for patients with or at risk of hepatocellular carcinoma (HCC).^{1,2} In the most recent version, published in 2018 (v2018), the LI-RADS M category (LR-M) represents observations that are probably or definitely malignant but not specific to HCC. However, based on current LI-RADS data, approximately one-third of all LR-M lesions are categorized as HCC, approximately two-thirds are categorized as non-HCC malignancies, and approximately 5% are categorized as benign.^{1,3} HCC with atypical features in the LR-M category should be diagnosed early to determine treatment options, as the biological behavior and prognoses differ between HCC and non-HCC malignancies.^{1,4} However, more importantly, distinguishing HCC from non-HCC malignancies remains extremely challenging,^{1,5} especially under the assumption that the presence of any LR-M features indicates LR-M. Due to the partial overlap between LR-M HCC and LR-M non-HCC malignancies with respect to the pathological components, clinical presentations, and imaging features, a biopsy is required for diagnosis.⁵⁻⁷ Additionally, imaging is usually required for guidance.⁵

For the diagnosis of HCC, multimodal imaging in cross-sections, especially dynamic contrast-enhanced magnetic resonance imaging (MRI), is one of the most effective tools due to the diagnostic information obtained from different MRI sequences.^{1,5,7,8} The LR-M diagnosis criteria are

composed of non-targetoid and targetoid masses. The latter represents intrahepatic cholangiocarcinoma (ICC), combined hepatocellular-cholangiocarcinoma, or HCC with atypical features. In addition, there are many other features, such as major and ancillary features, that favor HCC specifically or that are not included in LI-RADS.¹ Therefore, if support can be found for LR-M HCC in numerous features not restricted to LR-M criteria, it may not be necessary for some patients with a high risk of LR-M malignancies to undergo a biopsy. In this way, it may be possible to optimize the discrimination of HCC from non-HCC in LR-M lesions and to avoid significant complications by invasive tissue sampling. Following the identification of discriminative features, relative models were developed based on a variety of feature sets. Previous studies have focused on the discrimination of LR-M categories with different imaging features.⁹⁻¹³ However, few studies have proposed a non-invasive and comprehensive contrast-enhanced MRI model for the status of LR-M HCC with serology tests that are reasonably priced and readily available.

Based on these gaps in the literature, this study aimed to evaluate the predictive value of a combined model of MRI and clinicopathological features for identifying atypical HCC in LR-M observations.

Methods

Training patients

The protocol for this retrospective study was approved by the Shanghai General Hospital Institutional Review Board [(2023) 171, 5/16/2023] of the two hospitals in the study, and the requirement for informed consent was waived. A total of 375 consecutive patients were first identified from the first center [Hospital-1, Shanghai General Hospital-North (city center)] between December 2016 and November 2020. The inclusion criteria based on the LI-RADS v2018 diagnostic algorithm were as follows: (a) adult patients (≥ 18 years old), (b) patients with cirrhosis and/or chronic hepatitis B viral infection, (c) patients who had undergone a preoperative contrast-enhanced MRI within 3 weeks before surgery or biopsy, and (d) patients with LR-M features based on MRIs.¹ A total of 160 patients without eligible clinical and imaging data were excluded for the following reasons: (a) they had prior hepatic malignancies ($n = 25$), (b) important clinical data relating to them, such as levels of alpha-fetoprotein (AFP), carbohydrate antigen-199, carcinoem-

bryonic antigen, and aspartate aminotransferase (AST) were not available ($n = 78$), (c) they had received oncological treatment before undergoing MRI ($n = 50$), or (d) their MRI were of insufficient quality ($n = 7$), including 5 patients without the optimal timing arterial phase. Additionally, after imaging analysis, 110 patients were excluded for the following reasons: (e) they had coexisting LR-4 (probable HCC) and/or LR-5 (definite HCC) lesions ($n = 78$) for the reason that there was no way to determine either LR-M lesions or the coexisting LR-4 and/or LR-5 lesions contributing to serum tumor marker levels, (f) they had tumors in the vein ($n = 30$), or (g) they had cirrhosis due to a vascular disorder or diffuse nodular regenerative hyperplasia based on LI-RADS v2018 ($n = 2$). Ultimately, 105 patients were included in the study, and each patient was categorized into the LR-M HCC group ($n = 43$) or the non-HCC group ($n = 62$) (Figure 1).

Magnetic resonance image acquisition

All MRI abdominal images were obtained on a 3.0-Tesla clinical scanner [Philips Ingenia (Philips Healthcare) or General Electrical (GE) Discovery 750W (GE Healthcare)] using a body phased-array coil. The conventional abdominal MRI protocol consisted of the following sequences: T1-weighted (in-phase and out-of-phase), T2-weighted, and diffusion-weighted imaging (DWI) ($b = 0, 500, 1,000$ s/mm²). Corresponding maps of the apparent diffusion coefficient (ADC) were automatically calculated by the MRI system. For dynamic contrast-enhanced imaging, a three-dimensional gradient echo sequence with T1 high-resolution isotropic volume examination or liver acquisition with volume acceleration was performed before and after intravenous injection of gadopentetate dimeglumine. The contrast media (Magnevist; Bayer Healthcare, Germany, 0.1 mmol/kg) was injected at a rate of 1–2 mL/sec followed by a flush with a maximum dose of 20 mL saline. Hepatic arterial (early and late), portal, and equilibrium phase images were obtained at 15–25, 60–80, and 180 sec after contrast medium injection, respectively. The hepatobiliary agents were not used for abdominal MRI. Detailed MRI scanner parameters are shown in Supplementary Table 1.

Imaging analysis

All MRIs were assessed using the same picture archiving and communication system (Pacspeed, GE Medical Systems Integrated Imaging Solutions, Prospect, IL). An analysis of the images was performed independent-

Main points

- This retrospective study of 113 hepatocellular carcinomas (HCCs) at dynamic-enhanced magnetic resonance imaging (MRI) evaluated the predictive value to identify Liver Imaging Reporting and Data System (LI-RADS) M (LR-M) HCC in a combination model incorporating LI-RADS-based MRI and clinicopathologic features.
- In the combined model, aspartate aminotransferase >40 U/L [odds ratio (OR): 4.65], alpha-fetoprotein >20 ng/mL (OR: 13.04), surface retraction (OR: 0.16), enhancing capsule (OR: 5.24), blood products in mass (OR: 8.2) and iso/hypoenhancement on delayed phase (OR: 10.26) were independent predictors of LR-M HCC.
- The nomogram-based model had satisfactory performance to discriminate LR-M HCC from LR-M non-HCC (area under the curve: 0.95 for the training set and 0.90 for the validation set).

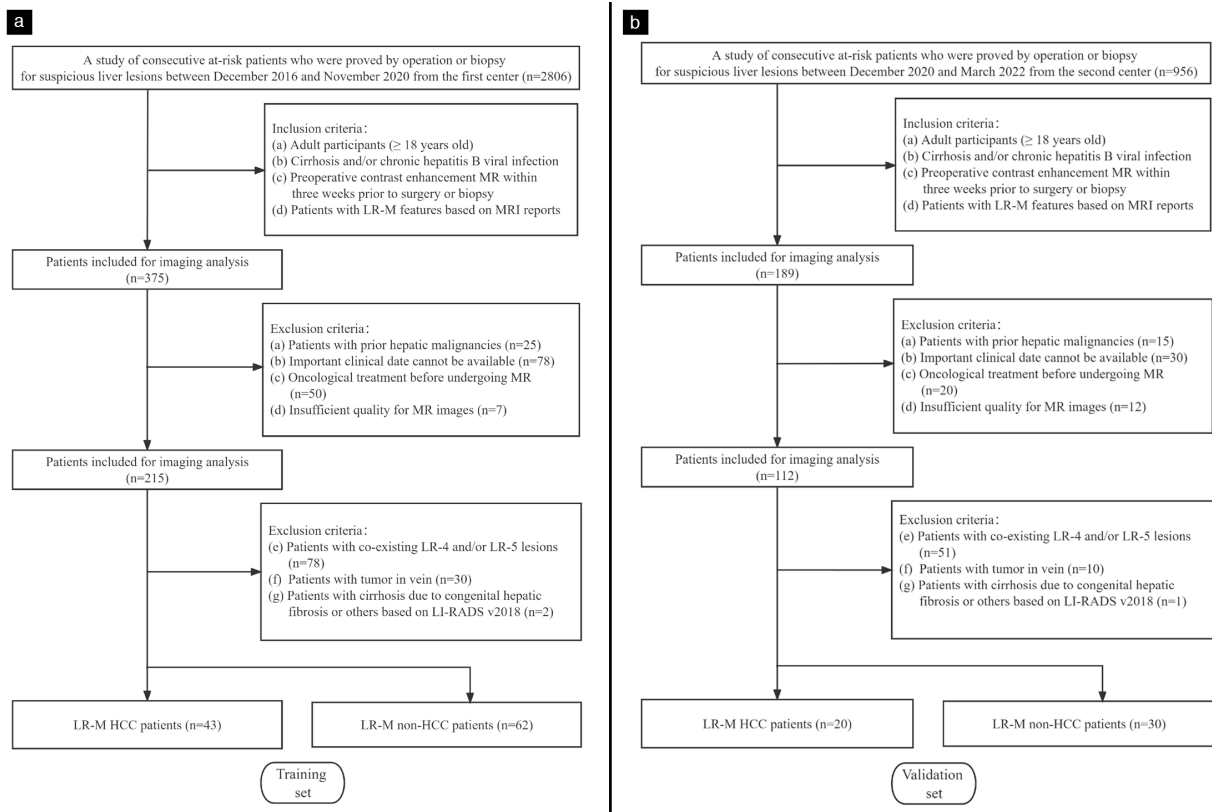


Figure 1. A flowchart illustrating the inclusion and exclusion criteria used in enrolling our Liver Imaging Reporting and Data System M observations of training (a) and validation (b) sets. LR-4, probable HCC; LR-5, definite HCC; LI-RADS v2018, LI-RADS version published in 2018; HCC, hepatocellular carcinoma; LI-RADS, Liver Imaging Reporting and Data System.

Table 1. The clinicopathologic characteristics of training and validation patients

Characteristics	Training patients		P value	Comparison with validation patients		
	HCC group	Non-HCC group		Training set	Validation set	P value
No. of patients*	43 (40.95)	62 (59.05)		105	50	
Sex* (no. of male/female)	31 (72.09)/12 (27.91)	46 (74.19)/16 (25.81)	0.682	77 (73.33)/28 (26.67)	36 (72)/14 (28)	0.141
Mean age (years) [^]	57 ± 14	63 ± 13	0.034	61 ± 14	59 ± 13	0.182
Etiology of liver disease*			1.000			0.262
Hepatitis B virus	41 (95.35)	57 (91.94)		98 (93.33)	47 (94)	
Hepatitis C virus	1 (2.33)	0 (0)		1 (0.95)	0 (0)	
Alcoholic liver disease	0 (0)	1 (1.61)		1 (0.95)	0 (0)	
None or other virus	1 (2.33)	4 (6.45)		5 (4.76)	3 (6)	
Cirrhosis*	25 (58.14)	23 (37.10)	0.146	48 (45.71)	21 (42)	0.431
Blood tests						
Total bilirubin level (umol/L) [#]	18.0 (6.0–76.0)	14.7 (6.3–119.5)	0.206	16.0 (6.0–119.5)	18.0 (32.1–151.0)	0.986
Albumin level (g/L) [^]	38.6 ± 5.2	38.6 ± 7.7	0.994	38.6 ± 6.8	36.6 ± 6.1	0.098
AST level (U/L)* (≤40/>40)	24 (51.06)/23 (48.94)	55 (83.33)/11 (16.67)	0.002	79 (69.91)/34 (30.09)	36 (67.92)/17 (32.08)	>0.999
ALT level (U/L)* (≤50/>50)	30 (63.83)/17 (36.17)	50 (75.76)/16 (24.24)	0.169	80 (70.80)/33 (29.20)	39 (73.58)/14 (26.42)	>0.999
Alkaline phosphatase level (U/L) [#]	87.0 (35.0–215.0)	99.6 (27.0–354.0)	0.625	90.0 (27.0–354.0)	81.0 (29.0–300.0)	0.613
Blood platelet level (x10 ⁹ /L) [^]	174.0 ± 84.6	182.5 ± 62.6	0.539	179.0 ± 72.4	181.4 ± 79.6	0.695
Serum tumor markers*						
AFP (ng/mL) (≤20/>20)	20 (42.55)/27 (57.45)	57 (86.36)/9 (13.64)	<0.001	77 (68.14)/36 (31.86)	32 (60.38)/21 (39.62)	0.972
CA19-9 (U/mL) (≤37/>37)	37 (78.72)/10 (21.28)	44 (66.67)/22 (33.33)	0.161	81 (71.68)/32 (28.32)	39 (73.58)/14 (26.42)	0.494
CEA (μg/mL) (≤5/>5)	41 (87.23)/6 (12.77)	45 (68.18)/21 (31.82)	0.019	86 (76.11)/27 (23.89)	43 (81.13)/10 (18.87)	0.969
Pathologic diagnosis*			0.447			0.088

Table 1. Continued

Characteristics	Training patients		<i>P</i> value	Comparison with validation patients		
	HCC group	Non-HCC group		Training set	Validation set	<i>P</i> value
HCC	47 (100)	0 (0)		47 (41.59)	20 (37.74)	
Non-HCC malignancies	ND	56 (84.85)		56 (49.56)	32 (60.38)	
ICC	ND	34 (51.52)			27 (50.94)	
cHCC-CCA	ND	7 (16.67)			2 (3.77)	
Metastasis	ND	10 (15.15)			2 (3.77)	
Other primary liver malignancies	ND	5 (7.58)			1 (1.89)	
Benign lesions*	ND	10 (15.15)		10 (8.85)	1 (1.89)	
No. of LR-M observations	47	66	0.714	113	53	
One/two	39 (90.70)/4 (9.30)	58 (93.55)/4 (6.45)		97 (92.38)/8 (7.62)	47 (94)/3 (6)	
Maximum diameter of tumor (mm) [#]	46.0 (12.0–148.0)	56.5 (12.0–76.0)	0.616	52.0 (12.0–176.0)	38.0 (5.0–106.6)	0.747
Subgroup (mm)* (<20/≥20)	7 (14.89)/40 (85.11)	5 (7.58)/61 (92.42)	0.350	12 (10.62)/101 (89.38)	7 (13.21)/46 (86.79)	>0.999
MRI morphology type*			0.205			0.995
Round or oval	20 (42.55)	30 (45.45)		50 (44.25)	27 (50.94)	
Round or oval with focal protrusions	6 (12.77)	2 (3.03)		8 (6.19)	4 (7.55)	
Lobulated	4 (8.51)	10 (15.15)		14 (12.39)	5 (9.43)	
Irregular growth	17 (36.17)	24 (36.36)		41 (36.28)	17 (32.08)	

All *P* values less than 0.05 are bold. Except where indicated, data are the number of patients or observations. *Numbers in parentheses are percentages; [^]data are means ± standard deviations; [#]data are median (min–max). ND, stands for not done; No., number of training or validation patients; AST, aspartate aminotransferase; ALT, alanine aminotransferase; AFP, alfa-fetoprotein; CA19-9, carbohydrate antigen 19-9; CEA, carcinoembryonic antigen; HCC, hepatocellular carcinoma; ICC, intrahepatic cholangiocarcinoma; cHCC-CCA, combined HCC-cholangiocarcinoma; MRI, magnetic resonance imaging.

ly by two abdominal radiologists, X-X.H. and L.Z., who had 7 and 23 years of experience in hepatic imaging, respectively. They were both blinded to any outcome information of patients, and disagreements were resolved by discussion based on bookmarked images, which were used as a guide.

The MRI morphological features were evaluated according to the LI-RADS v2018, including major, ancillary, and LR-M signs. The threshold growth was not included because there was only one examination per patient in the analysis. Moreover, the MRI signal intensity was evaluated at T1-weighted, T2-weighted, DWI, and postcontrast phase for the whole observation. Furthermore, the enhancement pattern of each observation was evaluated at the postcontrast phase. To avoid the influence of variable internal nodules, compartments, or septations on signal intensity in mosaic architecture, the hyper/iso/hypo signal intensity was defined as >50% of the whole observation showing visually assessed hyper/iso/hypo signal in the dynamic enhancement MRI and DWI within an observation.

Model building

First, for LR-M HCC, screening the risk factors consisting of clinicopathology and MRI

was performed using univariate analysis. Second, the least absolute shrinkage and selection operator (LASSO) regression was used for further screening of the selected variables to discourage the use of overfit data in the model. Additionally, as a result of constraints, those variables with a prevalence (<5% or >95%) were also discarded, considering their limited application in identifying different LR-M observations to ease model overfitting. Finally, a binary logistic regression analysis was conducted with backward stepwise selection. Variables with *P* values <0.05 were recognized as potential risk factors for LR-M HCC, and corresponding models were simultaneously established (Figure 2).

Validation patients

Another retrospective validation study consisting of 50 patients from the second center [Hospital-2, Shanghai General Hospital-South (Songjiang new city)] between December 2020 and March 2022 was available to verify the proposed predictive model. Patients were included and excluded using the same criteria as those in the training set, which were then used to validate (Figures 1, 2).

Statistical analysis

The descriptive statistics of data were given as mean ± standard deviation for nor-

malized variables and median (min–max) for non-normalized variables after a normality analysis of continuous variables using the Shapiro–Wilk test. For the categorical variables, descriptive statistics were reported as numbers and percentages (n, %). Continuous variables were compared using Student’s *t*-test or the Mann–Whitney *U* test. Categorical variables were analyzed with the χ^2 test or Fisher’s exact test where applicable. Univariate analysis and LASSO regression analysis were performed to identify the risk factors to discriminate LR-M HCC and LR-M non-HCC. Binary logistic regression analysis was then conducted to build clinicopathologic, MRI, and combined models. Receiver operating characteristics (ROC) analysis was finally performed with corresponding areas under the curve (AUCs) computed. Inter-observer agreement analysis for MRI features was performed using Cohen’s kappa statistics (slight, 0.00–0.20; fair, 0.21–0.40; moderate, 0.41–0.60; substantial, 0.61–0.80; perfect, 0.81–1.00). Values of *P* < 0.05 were considered statistically significant. All data analyses were performed using MedCalc software (MedCalc 20.022; MedCalc, Mariakerke, Belgium) and R software (version 3.4.1).

Results

Clinicopathologic characteristics

A total of 105 patients (mean age, 61 ± 14 years; 77 men) with 113 liver observations were classified as the training set, which comprised 47 (41.59%) LR-M HCC malignancies, 56 (49.56%) LR-M non-HCC malignancies, and 10 (8.85%) benign lesions. Seven patients were diagnosed by biopsy, and each patient had one observation. A total of 50 patients (mean age, 59 ± 13 years; 36 men) with

53 liver observations were classified as the validation set. The training set comprised an HCC group (mean age, 57 ± 14 years; 31 men, 12 women) and a non-HCC group (mean age, 63 ± 13 years; 46 men, 16 women) ($P = 0.03$). There was no significant difference between the sex distributions of the two groups ($P = 0.682$), but there was a statistically significant difference in the ages of the two groups ($P = 0.034$). In the training set, hepatitis B virus infection was observed in most patients, whether in the HCC group [41 (95.35%)] or in the non-HCC group [57 (91.94%)], where-

as other etiologies occurred rarely. The AST levels >40 U/L and serum AFP levels >20 ng/mL were both significantly higher ($P = 0.002$, $P < 0.001$, respectively) in the HCC group [23 (48.94%); 27 (57.45%)] than in the non-HCC group [11 (16.67%); 9 (13.64%)]. However, serum carcinoembryonic antigen levels ≤ 5 μ g/mL were more likely to be lower in the HCC group [41 (87.23%)] than in the non-HCC group [45 (68.18%)] ($P = 0.019$). There were no significant differences in the remaining demographic variables between the two groups. Additionally, no variables were significantly different between the training and validation sets. An overview of the data is presented in Table 1.

Univariate analysis of magnetic resonance imaging features

The MRI features of the LR-M HCC and non-HCC groups are summarized in Table 2. Fifteen MRI features remained after univariate analysis. For the LR-M targetoid appearance, 14 (29.79%) cases had peripheral washout in the HCC group compared with 6 (9.09%) in the non-HCC group ($P = 0.004$), whereas only 3 (6.38%) cases had delayed central enhancement in the HCC group compared with 16 (24.24%) cases in the non-HCC group ($P = 0.012$). For LR-M nontargetoid appearance, marked diffusion restriction [11 (23.40%) cases], surface retraction [6 (12.77%) cases] and peritumoral bile duct dilatation [5 (10.64%) cases] were less frequent in the HCC group than in the non-HCC group [28 (42.42%), 32 (48.48%), and 29 (43.94%) cases, respectively] ($P = 0.036$, $P < 0.001$, $P < 0.001$, respectively). In regard to major features, capsular enhancement was more frequent in the HCC group [25 (53.19%) cases] than in the non-HCC group [15 (22.73%) cases] ($P = 0.001$). Regarding the ancillary features favoring HCC, all variables were significantly different between the two groups. For the signal intensity and enhancement pattern, washout or isoenhancement on the portal venous or delayed phase (DP) was present among 21 cases in the HCC group (44.68%) and only 4 cases in the non-HCC group (6.06%) ($P < 0.001$). Hyperenhancement was not significantly more common in the portal venous phase or DP in the HCC group than in the non-HCC group. The hyperintensity on DWIs constituted the majority of observations in both groups, with $P = 0.016$.

Feature selection

The results of the selection algorithm are detailed in Figure 2. A total of 19 variables related to clinicopathology and MRI met the

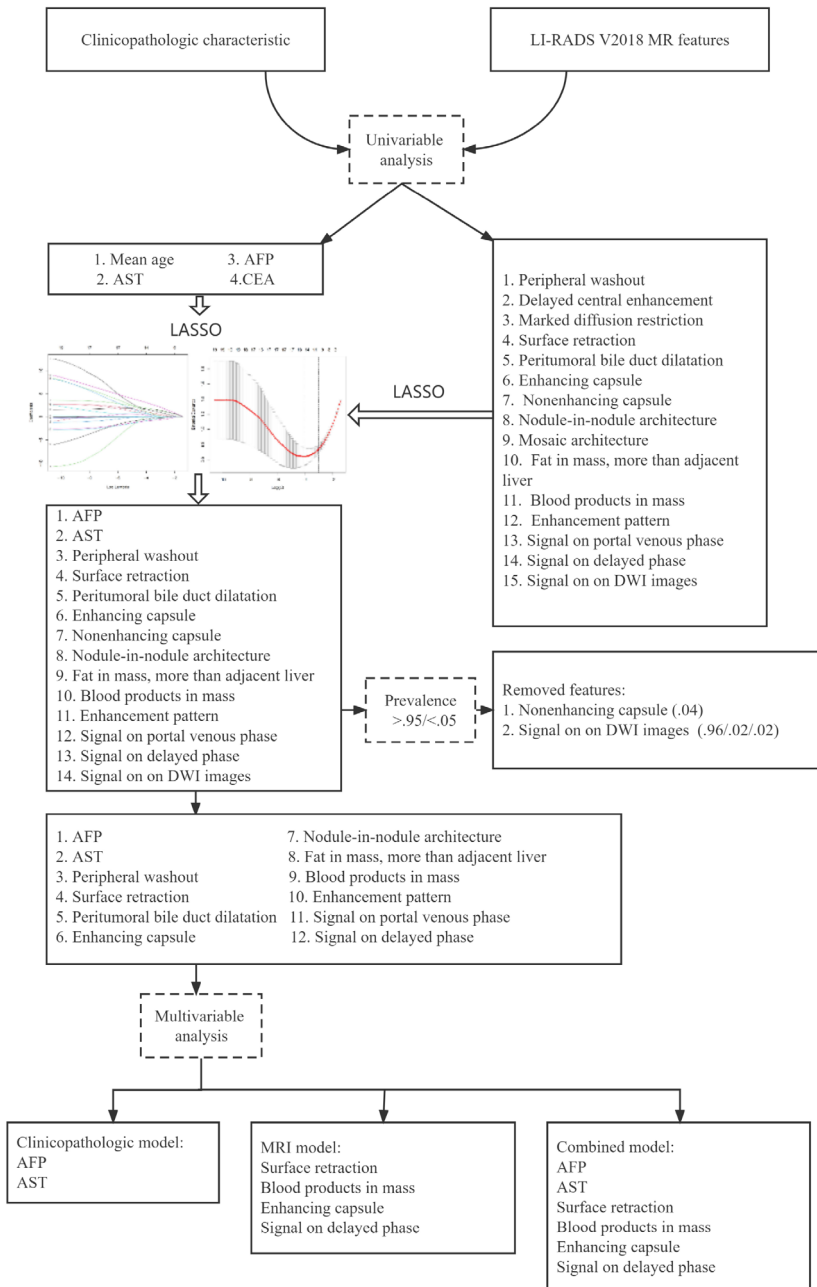


Figure 2. A workflow for creating clinicopathologic, MRI, and combined diagnostic models identifying Liver Imaging Reporting and Data System M hepatocellular carcinoma. LI-RADS v2018, LI-RADS version published in 2018; AFP, alpha-fetoprotein; AST, aspartate aminotransferase; CEA, carcinoembryonic antigen; LASSO, least absolute shrinkage and selection operator; DWI, diffusion-weighted imaging; MRI, magnetic resonance imaging; LI-RADS, Liver Imaging Reporting and Data System.

Table 2. MRI Features based on LI-RADS for identifying LR-M HCC and non-HCC: univariate analysis

MRI features	HCC group (n = 47)	Non-HCC group (n = 66)	Kappa value	Prevalence	P value
LR-M					
Targetoid appearance[^]					
Rim APHE	36 (76.60)	51 (77.27)	0.91		0.933
Peripheral washout	14 (29.79)	6 (9.09)	0.89	0.18	0.004
Delayed central enhancement	3 (6.38)	16 (24.24)	0.90	0.17	0.012
Targetoid restriction	15 (31.91)	22 (33.33)	0.84		0.874
Non-targetoid appearance[^]					
Infiltrative appearance	20 (42.55)	24 (36.36)	0.78		0.506
Marked diffusion restriction	11 (23.40)	28 (42.42)	0.86	0.35	0.036
Necrosis or severe ischemia	16 (34.04)	21 (31.82)	0.80		0.804
Surface retraction	6 (12.77)	32 (48.48)	0.95	0.34	<0.001
Peritumoral bile duct dilatation	5 (10.64)	29 (43.94)	0.87	0.30	<0.001
Major features[^]					
Non-rim APHE	5 (10.64)	3 (4.55)	0.81		0.274
Non-peripheral washout	1 (2.13)	0 (0)	0.67		0.416
Enhancing capsule	25 (53.19)	15 (22.73)	0.92	0.35	0.001
Ancillary features[^]					
Favoring HCC					
Non-enhancing capsule	5 (10.64)	0 (0)	0.70	0.04	0.011
Nodule-in-nodule architecture	7 (14.89)	1 (1.52)	0.81	0.07	0.009
Mosaic architecture	16 (34.04)	10 (15.15)	0.88	0.23	0.019
Fat in mass, more than adjacent liver	15 (31.91)	0 (0)	0.96	0.13	<0.001
Blood products in mass	19 (40.43)	6 (9.09)	0.91	0.22	<0.001
Favoring malignancy					
Corona enhancement	7 (14.89)	17 (25.76)	0.81		0.164
Fat sparing in solid mass	2 (4.26)	4 (6.06)	0.79		1.000
Iron sparing in solid mass	1 (2.13)	1 (1.52)	0.72		1.000
Restricted diffusion	46 (97.87)	65 (98.48)	0.95		1.000
Mild-moderate T2 hyperintensity	42 (89.36)	57 (86.36)	0.96		0.634
Other features					
Enhancement pattern [^]			0.80		<0.001
Progressive or persistent/washout or iso enhancement on PVP or DP	26 (55.32)/21 (44.68)	62 (93.94)/4 (6.06)		0.78/0.22	
Signal intensity on AP [^] Hyper/(iso/hypo)	40 (85.11)/7 (14.89)	56 (84.85)/10 (15.15)	0.97		0.97
Signal intensity on PVP [^] Hyper/(iso/hypo)	26 (55.32)/21 (44.68)	56 (84.85)/10 (15.15)	0.93	0.73/0.27	0.001
Signal intensity on DP [^] Hyper/(iso/hypo)	21 (44.68)/26 (55.32)	59 (89.39)/7 (10.61)	0.91	0.71/0.29	<0.001
Signal intensity on T1-weighted images* Hyper/iso/hypo	3 (6.38)/2 (4.26)/42 (89.36)	1 (1.52)/3 (4.55)/62 (93.94)	0.96		0.355
Signal intensity on T2-weighted images* Hyper/iso/hypo	44 (93.62)/2 (4.26)/1 (2.13)	64 (96.97)/2 (3.03)/0 (0)	0.96		0.299
Signal intensity on DWI images* Hyper/iso/hypo	43 (91.49)/2 (4.26)/2 (4.26)	66 (100)/0 (0)/0 (0)	0.90	0.96/0.02/0.02	0.016

All P values less than 0.05 are bold. Data are numbers of observations, with percentages in parentheses. [^]Chi-square test; *Mann-Whitney U test; LI-RADS, Liver Imaging Reporting and Data System; HCC, hepatocellular carcinoma; APHE, arterial phase hyperenhancement; PVP, portal venous phase; DP, delayed phase; AP, arterial phase; DWI, diffusion-weighted imaging; MRI, magnetic resonance imaging.

criteria for univariate analysis. By performing a LASSO regression analysis, 14 variables with non-zero coefficients were then entered into the training set (λ : 0.017655622). Finally, two variables (non-enhancing capsule and signal on DWIs) were removed from the model due to the prevalence being too high or low.

Multivariate analysis

Detailed results are presented in Table 3. The diagnostic model of LR-M HCC based on only clinicopathological characteristics showed that both AST [odds ratio (OR): 6.72; 95% confidence interval (CI): 2.44, 18.49; $P < 0.001$] and AFP (OR: 11.19; 95% CI: 4.05, 30.90; $P < 0.001$) were significant risk factors for

HCC. The second model based on only MRI features showed that surface retraction (OR: 0.11; 95% CI: 0.03, 0.40; $P < 0.001$), capsular enhancement (OR: 6.69; 95% CI: 2.13, 21; $P = 0.001$), blood products in mass (OR: 6.25; 95% CI: 1.7, 23; $P = 0.006$), and iso/hypoenhancement on DP (OR: 12.76; 95% CI: 3.67, 44.36; $P < 0.001$) were significant risk factors for HCC. The combined model consisting of clinicopathological and MRI factors showed that all of the abovementioned variables with different ORs and 95% CIs were associated with HCC (Figure 3). As a final step, a forest plot and nomogram were developed after identifying those factors.

Diagnostic performance of different models from the training and validation sets

An assessment of diagnostic test results using ROC curve analysis was further performed to identify LR-M HCC for different models (Figure 4). The AUCs with 95% CIs were 0.81 (0.72, 0.88), 0.89 (0.81, 0.94), and 0.95 (0.89, 0.98) for the clinicopathological model, MRI model, and combined model in the training set, respectively. The AUCs with 95% CIs were 0.74 (0.61, 0.85), 0.88 (0.76, 0.95), and 0.90 (0.76, 0.97) for the clinicopathological model, MRI model, and combined model in the validation set, respectively. The corresponding sensitivities, specificities, positive predictive values, negative predictive values, positive likelihood ratios, negative likelihood ratios, and cut-off values are detailed in Table 4.

Prediction of the nomogram and construction of external validation

A ROC curve was also drawn to assess the diagnostic accuracy of LR-M HCC in the validation set (Figure 4). The AUC value of the combined model [OR (95% CI), 0.90 (0.76,

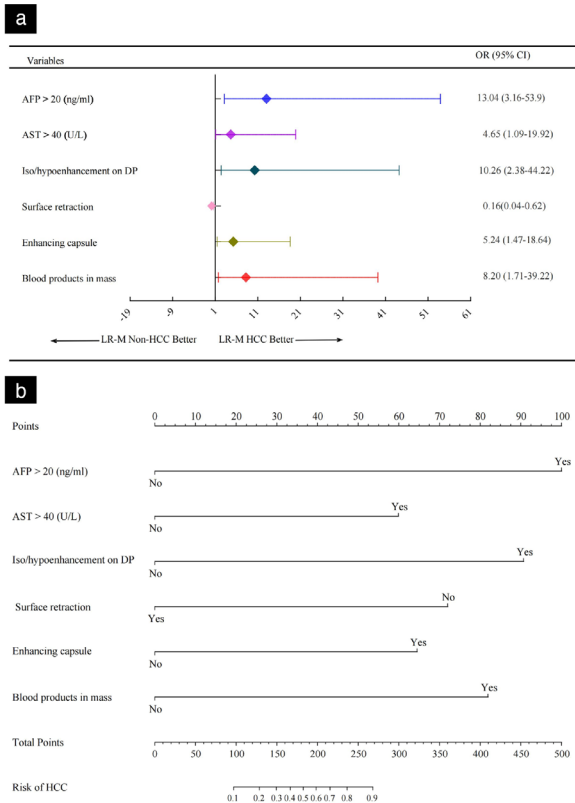


Figure 3. A forest plot (a) used to display the prognostic factors of the Liver Imaging Reporting and Data System (LI-RADS) M (LR-M) hepatocellular carcinoma (HCC) in the combined model. A nomogram (b) for predicting the LR-M HCC probabilities based on the combined model. The points were obtained by drawing a vertical line from the single variable axis to the point axis for each factor. The total points were then projected onto the bottom axis to obtain a personalized probability of LR-M HCC risk. AFP, alpha-fetoprotein; AST, aspartate aminotransferase; DP, delayed phase; HCC, hepatocellular carcinoma; OR, odds ratio; CI, confidence interval.

Table 3. Clinicopathologic and MRI features associated with LR-M HCC: binary logistic regression analysis

Features	Clinicopathologic model		MRI model		Combined model	
	OR (95% CI)	P value	OR (95% CI)	P value	OR (95% CI)	P value
Clinicopathologic						
AST (>40)*	6.72 (2.44, 18.49)	0.002			4.65 (1.09, 19.92)	0.038
AFP (> 20)*	11.19 (4.05, 30.90)	<0.001			13.04 (3.16, 53.90)	<0.001
MRI						
Surface retraction (non)*			0.11 (0.03, 0.40)	<0.001	0.16 (0.04, 0.62)	0.008
Enhancing capsule (no)^			6.69 (2.13, 21.00)	0.001	5.24 (1.47, 18.64)	0.012
Blood products in mass (non)*			6.25 (1.70, 23.00)	0.006	8.20 (1.71, 39.22)	0.008
Signal intensity on DP (iso/hypo)*			12.76 (3.67, 44.36)	<0.001	10.26 (2.38, 44.22)	0.002

*/^/Contents in parentheses are reference categories. Non/no stands for the negative of the variables. "No" refers to only no enhancing capsule, but not refers to non-enhancing capsule, which was removed from the analysis due to low prevalence. Hosmer and Lemeshow goodness of fit test was performed for the combined model with a P value of 0.370, illustrating no evidence of poor fit. LI-RADS M, Liver Imaging Reporting and Data System M; HCC, hepatocellular carcinoma; OR, odds ratio; CI, confidence intervals; AST, aspartate aminotransferase; AFP, alpha-fetoprotein; DP, delayed phase, MRI, magnetic resonance imaging.

0.97)] was greater than that of both the clinicopathological [0.74 (0.61, 0.85)] and MRI models [0.88 (0.76, 0.95)] in the validation set, similar to the results mentioned earlier

in the training set. Overall, the combined model had the strongest predictive value in both the training and validation sets, with a concordance index (C-index) of 0.948 and

0.899, respectively. As shown by the calibration plots (Figure 4), both the training and validation sets showed good consistency between the predictions and the actual obser-

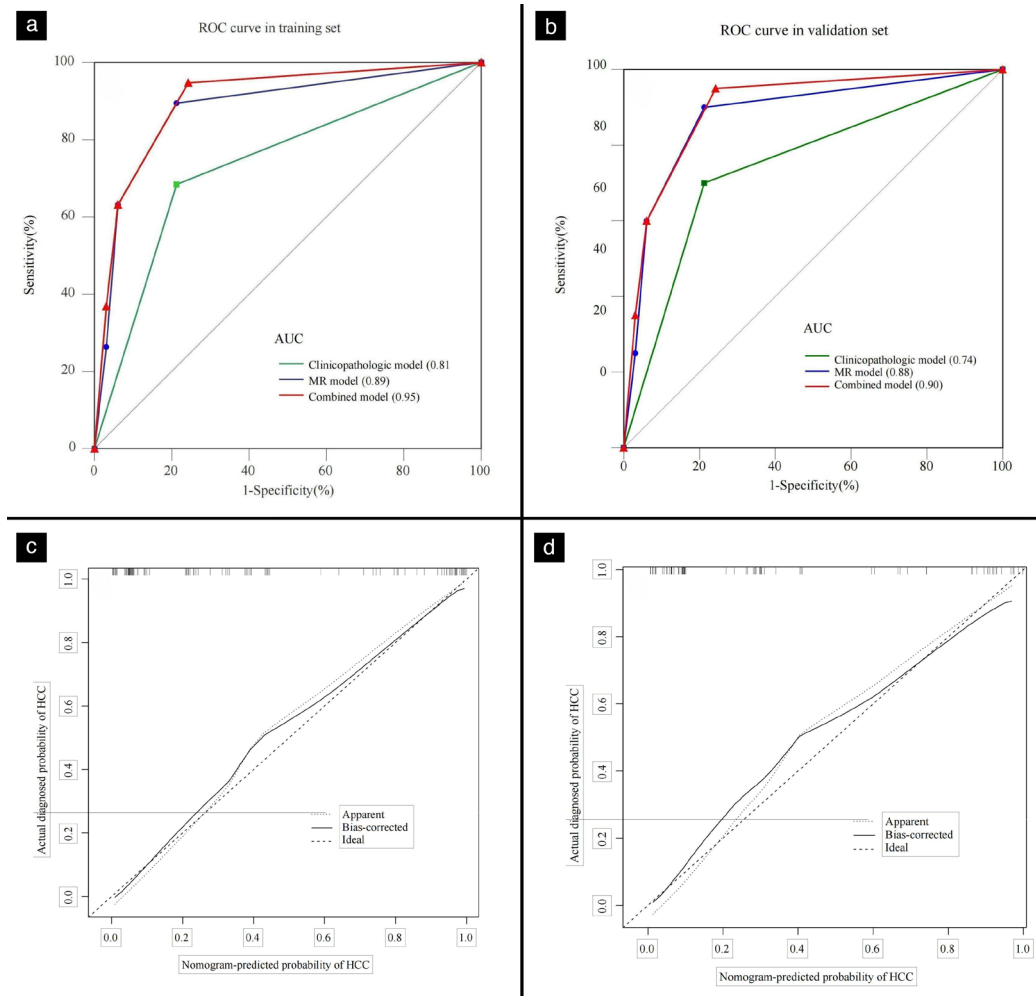


Figure 4. A receiver operating characteristic curve used to evaluate the diagnostic value for the Liver Imaging Reporting and Data System M hepatocellular carcinoma of clinicopathologic, MRI, and combined model in the training (a) and validation (b) sets. A calibration curve was used to evaluate the calibration performance of the combined model in the training (c) and validation (d) sets. ROC, receiver operating characteristic; AUC, area under the curve; HCC, hepatocellular carcinoma; MRI, magnetic resonance imaging.

Table 4. The diagnostic performance of the clinicopathologic, MRI, and combined model for identifying LR-M HCC and non-HCC

Model	Training patients			Validation patients		
	Clinicopathologic model	MRI model	Combined model	Clinicopathologic model	MRI model	Combined model
AUC (95% CI)	0.81 (0.72, 0.88)	0.89 (0.81, 0.94)	0.95 (0.89, 0.98)	0.74 (0.61, 0.85)	0.88 (0.76, 0.95)	0.90 (0.76, 0.97)
P value	<0.001	<0.001	<0.001	0.003	<0.001	<0.001
Sensitivity (95% CI)	83.0 (69.2, 92.4)	85.1 (71.7, 93.8)	93.6 (82.5, 98.7)	70.0 (45.7, 88.1)	90.0 (68.3, 98.8)	95.0 (75.1, 99.9)
Specificity (95% CI)	71.2 (58.7, 81.7)	84.9 (73.9, 92.5)	87.9 (77.5, 94.6)	78.8 (61.1, 91.0)	78.8 (61.1, 91.0)	75.8 (57.7, 88.9)
PPV (95% CI)	67.2 (57.9, 75.4)	80.0 (69.1, 87.8)	84.6 (74.1, 91.4)	66.7 (49.4, 80.4)	72.0 (56.7, 83.5)	70.4 (56.3, 81.4)
NPV (95% CI)	85.5 (75.4, 91.8)	88.9 (80.0, 94.1)	95.1 (86.6, 98.3)	81.2 (68.4, 89.6)	79.5 (69.2, 87.0)	96.2 (78.6, 99.4)
PLR (95% CI)	2.88 (1.93, 4.30)	5.62 (3.13, 10.1)	7.72 (4.02, 14.9)	3.3 (1.61, 6.76)	4.2 (2.16, 8.32)	3.92 (2.13, 7.22)
NLR (95% CI)	0.24 (0.12, 0.46)	0.18 (0.09, 0.35)	0.07 (0.02, 0.22)	0.38 (0.19, 0.76)	0.43 (0.25, 0.73)	0.07 (0.01, 0.45)
Cut-off value	0.15	0.24	0.33	0.19	0.10	0.07

LI-RADS M, Liver Imaging Reporting and Data System M; HCC, hepatocellular carcinoma; AUC, area under the curve; CI, confidence intervals; PPV, positive predictive value; NPV, negative predictive value; PLR, positive likelihood ratio; NLR, negative likelihood ratio; MRI, magnetic resonance imaging.

vations. The clinical use of decision curve analysis for the LR-M HCC nomogram is presented in Figure 5. Ultimately, two examples of a nomogram application in practice are presented in Figure 6.

Discussion

Recently, various prognostic models for LR-M lesions have been described,¹¹⁻¹⁵ but an ideal model combining clinicopathologic and MRI features for discriminating LR-M HCC from other observations has not been developed. In a previous study,¹² targetoid tumors and enhancing capsules were combined to identify LR-M HCC, which showed high specificity (93.8%) but low sensitivity (76.6%). In this study, the authors established a nomogram-based combined model including AST, AFP, and MRI (surface retraction, enhancing capsule, blood products in mass, and iso/hypo-enhancement on DP) features to classify LR-M HCC. The model had a high sensitivity (training, 93.6%; validation, 95%) for identifying LR-M HCC with specificity (training, 87.9%; validation, 75.8%). The nomogram

for identifying LR-M HCC yielded satisfactory results in the training (C-index 0.948) and validation (C-index 0.899) datasets.

High AFP levels [OR: 13.04; 95% CI: (3.16, 53.9)] had the strongest association with LR-M HCC and had the highest weight in the nomogram-based model. AFP levels played an important role in distinguishing LR-M HCC from other observations in previous studies,¹⁶⁻¹⁸ and AFP expression was also higher in cytokeratin 19-positive patients with HCC who were more coincident with imaging features for LR-M HCCs.^{13,19} Thus, AFP levels may be used to identify LR-M HCCs, but with the consideration that AFP levels were also high in patients with combined HCC-cholangiocarcinoma (cHCC-CCA). In our current study, cHCC-CCA was comprised of only 10.61% of LR-M non-HCC in the training set and only 6.06% in the validation set. A relatively small amount of cHCC-CCA may have had an impact on the significance of AFP. Therefore, discrimination between LR-M HCCs and LR-M non-HCCs based on AFP levels remains to be further confirmed in

a larger study. The AST levels [OR: 4.65; 95% CI, (1.09, 19.92)] were of minimal importance for our model, even though it was regarded as a predictor for LR-M HCC. It is possible that the microenvironment of the chronic inflammatory response of the liver and subsequent liver damage contributed to HCC,^{7,20,21} which resulted in clinically higher AST levels among patients with impaired hepatic function.

As the strongest contributor to the MRI model, iso/hypo-enhancement on DP [OR: 10.26; 95% CI, (2.38, 44.22)] ranked second only to AFP levels for identifying LR-M HCC in the combined model. Previous studies showed that hyperintensity on DP was more common in ICC than in atypical HCC.^{6,15} These findings were similar to the authors' findings that hyperintense lesions accounted for most LR-M non-HCC lesions (89.39%), of which more than half were ICC. The reason may be linked to the relatively abundant pathological fibrosis of ICC compared with LR-M HCC, which can mimic conventional HCC.^{22,23} On the contrary, sparing fibrosis in LR-M HCC makes a relatively weak contribution to the prolonged retention of extracellular gadolinium contrast agent, which results in iso-intense or hypointense on DP in LR-M HCC.

In addition to iso/hypo-enhancement on DP, both enhancing capsule [OR: 5.24; 95% CI: (1.47, 18.64)] and surface retraction [OR: 0.16; 95% CI, (0.04, 0.62)] were correlated with LR-M HCC. Enhancing capsule suggested more fibrous tissue peripherally, which represented expansile growth in atypical HCC.^{14,22} In contrast, more than half (51.52%) of the non-HCC cases in the study were ICC cases, which contained a higher proportion of tumor cells peripherally, manifesting an uncommon capsule appearance.²⁴ Although a small fraction of HCCs may mimic pathological findings of ICCs based on similar biliary differentiation,^{25,26} enhancing capsule still reliably predicted LR-M HCC. Conversely, surface retraction occurred less frequently [6/47 (12.77%)] in the LR-M patients with HCC. It is possible that surface retraction was frequently observed in mass-forming ICC with a relatively fibrotic component instead of HCC, as described in previous studies.^{15,27}

Blood products in mass [OR: 8.2; 95% CI, (1.71, 39.22)] was associated with LR-M HCC. This feature accounted for 40.43% of LR-M HCC lesions, similar to a 50% proportion reported by Jiang et al.¹³ Another study indicated that blood products in mass may be useful for differentiating LR-M HCC from non-HCC malignancies.²⁸ Usually, hemorrhage represents rapidly growing tumors

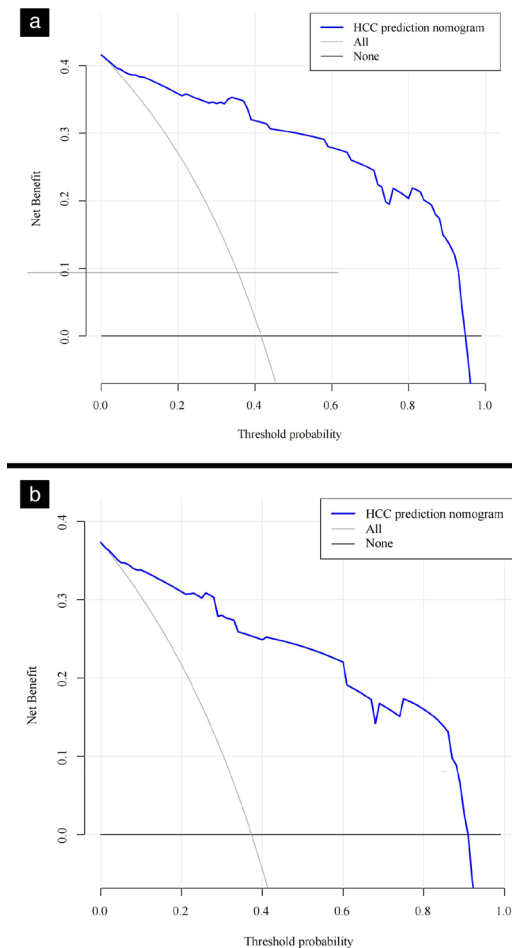


Figure 5. A decision curve analysis performed to characterize the potential decision thresholds in the training (a) and validation (b) sets. HCC, hepatocellular carcinoma.

with an increasing level of malignancy, and the tumor vasculature is correspondingly disrupted. Compared with conventional HCC, LR-M patients with HCC experienced a worse prognosis and were also characterized by abundant blood supply.^{19,25,29} This may

explain why LR-M HCC cases had a significantly higher incidence of blood products than non-HCC cases with a relatively insufficient blood supply.

The study's predictive model of LR-M HCC was developed using univariate, LASSO, and

multivariate analysis, which effectively enabled the feature selection. For the training cohort, the prediction model that contained six selected factors yielded an AUC of 0.95. The calibration curve results showed satisfactory agreement between the predicted LR-M HCC rates and observed probability. The validation of the nomogram-based model is crucial in avoiding overfitting and determining the generalization.³⁰ Thus, external experimental data were validated in our combined model. The AUC reached 0.90 for the validation set when distinguishing LR-M HCC and demonstrated a good calibration power in which the bias-corrected curve was close to the ideal curve. Additionally, the combined model with the decision curve provided more benefits for making clinical decisions within a range of 0.01–0.94 and 0.02–0.90 threshold probability in the training and validation sets, respectively. By using the nomogram-based model, clinicians can accurately predict the HCC risk of individuals with LR-M observations.

Several limitations were identified in this study. First, it was done retrospectively. Second, a relatively small sample was used in the multivariate analysis; however, another study demonstrated that relaxing the rule of ten events for one variable in logistic regression was acceptable in certain contexts.³¹ Third, the authors could not evaluate MRI features in the transitional and hepatobiliary phases without performing gadoteric acid-enhanced MR imaging due to medical insurance considerations. Fourth, a large prevalence of hepatitis B virus infection might limit the utility in Western countries. Fifth, there was a limited number of combined-type HCC-CCA lesions, which made it particularly challenging to differentiate LR-M observations. Sixth, patients diagnosed by biopsy may not exclude the possibility of cHCC-CCA, even though only seven patients were involved. Finally, it was not possible to perform quantitative measurements for ADC value and contrast-enhanced MRI parameters due to the use of different MRI scanners.

In conclusion, the overall analysis of this combined nomogram-based model incorporating clinicopathologic and MRI items demonstrated a satisfactory prediction result for LR-M HCC, and data are easily available via routine blood tests and MRI examination. The model may have substantial clinical utility not only in terms of individualized risk estimation but also in terms of its clinical application for minimizing or eliminating the need for biopsy.

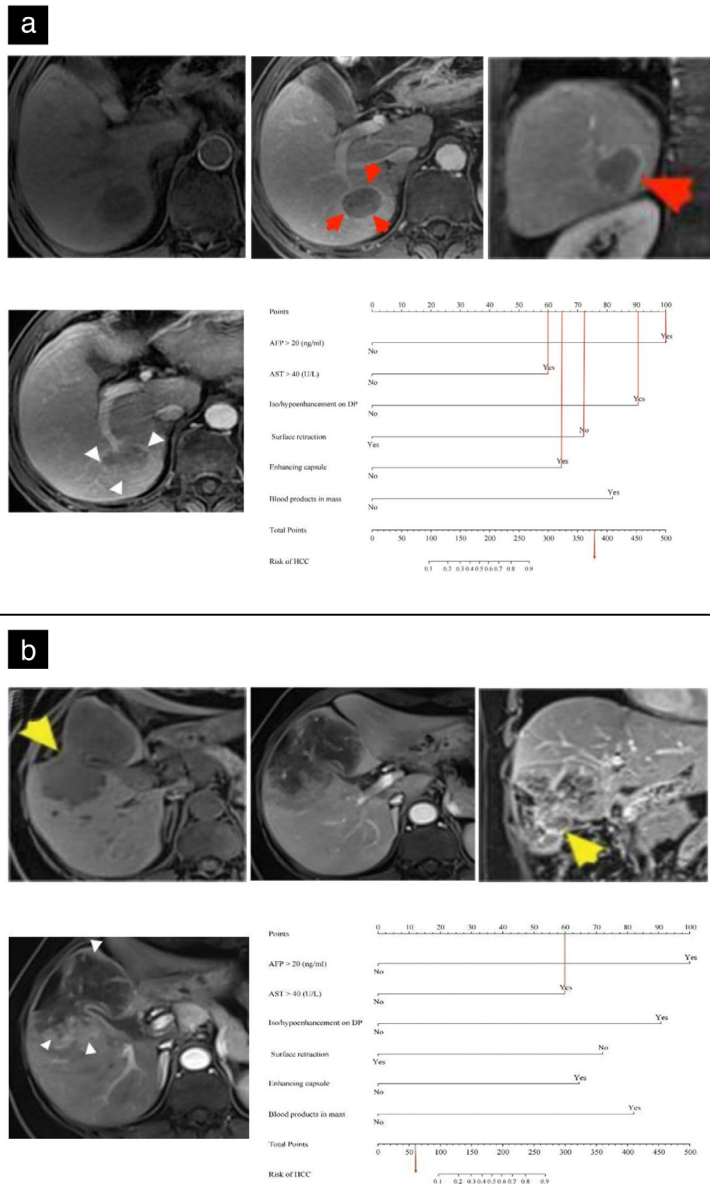


Figure 6. Illustration of the nomogram for clinical application. (a) Surgically confirmed hepatocellular carcinoma (HCC) with LI-RADS M (LR-M) features in a 60-year-old man who had an aspartate aminotransferase (AST) level of 120 U/L and an alpha-fetoprotein (AFP) level of 300 ng/mL. The tumor showed no blood products sign on precontrast T1-weighted imaging (top, left), slight hyperenhancement (white arrow) peripherally on arterial phase (bottom, left), enhancing capsule (red arrow) on both portal venous phase (top, middle) and coronal delayed phase (top, right), hypoenhancement on coronal delayed phase (top, right), and no surface retraction sign on all images. Total points of 388 represented an LR-M HCC risk >0.9 (bottom, right). (b) Surgically confirmed intrahepatic cholangiocarcinoma with LR-M features in a 55-year-old woman who had an AST level of 80 U/L and an AFP level of 12 ng/mL. The tumor showed no blood products sign on precontrast T1-weighted imaging (top, left), heterogeneous hyperenhancement peripherally (white arrow) on arterial phase (bottom, left), no enhancing capsule on both portal venous phase (top, middle) and coronal delayed phase (top, right), heterogeneous hyperenhancement on coronal delayed phase (top, right) and surface retraction (yellow arrow) on precontrast T1-weighted imaging (top, left) and coronal delayed phase (top, right). Total points of 60 represented an LR-M non-HCC risk of <0.1 (bottom, right).

Conflict of interest disclosure

The authors declared no conflicts of interest.

References

1. American College of Radiology. Liver Imaging reporting and data system version 2018. [\[CrossRef\]](#)
2. Cerny M, Bergeron C, Billiard JS, et al. LI-RADS for MR imaging diagnosis of hepatocellular carcinoma: performance of major and ancillary features. *Radiology*. 2018;288(1):118-128. [\[CrossRef\]](#)
3. Tang A, Singal AG, Mitchell DG, et al. Introduction to the Liver Imaging Reporting and Data System for Hepatocellular Carcinoma. *Clin Gastroenterol Hepatol*. 2019;17(7):1228-1238. [\[CrossRef\]](#)
4. Torimura T, Iwamoto H. Treatment and the prognosis of hepatocellular carcinoma in Asia. *Liver Int*. 2022;42(9):2042-2054. [\[CrossRef\]](#)
5. Marrero JA, Kulik LM, Sirlin CB, et al. Diagnosis, staging, and management of hepatocellular carcinoma: 2018 practice guidance by the American Association for the Study of Liver Diseases: Marrero et al. *Hepatology*. 2018;68(2):723-750. [\[CrossRef\]](#)
6. Rimola J, Forner A, Reig M, et al. Cholangiocarcinoma in cirrhosis: absence of contrast washout in delayed phases by magnetic resonance imaging avoids misdiagnosis of hepatocellular carcinoma. *Hepatology*. 2009;50(3):791-798. [\[CrossRef\]](#)
7. Llovet JM, Kelley RK, Villanueva A, et al. Hepatocellular carcinoma. *Nat Rev Dis Primers*. 2021;7(1):6. [\[CrossRef\]](#)
8. Davenport MS, Khalatbari S, Liu PSC, et al. Repeatability of diagnostic features and scoring systems for hepatocellular carcinoma by using MR imaging. *Radiology*. 2014;272(1):132-142. [\[CrossRef\]](#)
9. Kim DH, Choi SH, Park SH, et al. Liver imaging reporting and data system category M: a systematic review and meta-analysis. *Liver Int*. 2020;40(6):1477-1487. [\[CrossRef\]](#)
10. Shin J, Lee S, Hwang JA, et al. MRI-diagnosis of category LR-M observations in the Liver Imaging Reporting and Data System v2018: a systematic review and meta-analysis. *Eur Radiol*. 2022;32(5):3319-3326. [\[CrossRef\]](#)
11. Jang JK, Choi SH, Byun JH, et al. New strategy for Liver Imaging Reporting and Data System category M to improve diagnostic performance of MRI for hepatocellular carcinoma ≤ 3.0 cm. *Abdom Radiol (NY)*. 2022;47(7):2289-2298. [\[CrossRef\]](#)
12. Min JH, Kim JM, Kim YK, et al. A modified LI-RADS: targetoid tumors with enhancing capsule can be diagnosed as HCC instead of LR-M lesions. *Eur Radiol*. 2022;32(2):912-922. [\[CrossRef\]](#)
13. Jiang H, Song B, Qin Y, et al. Diagnosis of LI-RADS M lesions on gadoxetate-enhanced MRI: identifying cholangiocarcinoma-containing tumor with serum markers and imaging features. *Eur Radiol*. 2021;31(6):3638-3648. [\[CrossRef\]](#)
14. Min JH, Kim YK, Choi SY, et al. Differentiation between cholangiocarcinoma and hepatocellular carcinoma with target sign on diffusion-weighted imaging and hepatobiliary phase gadoxetic acid-enhanced MR imaging: classification tree analysis applying capsule and septum. *Eur J Radiol*. 2017;92:1-10. [\[CrossRef\]](#)
15. Sheng RF, Zeng MS, Rao SX, Ji Y, Chen LL. MRI of small intrahepatic mass-forming cholangiocarcinoma and atypical small hepatocellular carcinoma (≤ 3 cm) with cirrhosis and chronic viral hepatitis: a comparative study. *Clin Imaging*. 2014;38(3):265-272. [\[CrossRef\]](#)
16. Galle PR, Foerster F, Kudo M, et al. Biology and significance of alpha-fetoprotein in hepatocellular carcinoma. *Liver Int*. 2019;39(12):2214-2229. [\[CrossRef\]](#)
17. Huang JY, Li JW, Ling WW, et al. Can contrast enhanced ultrasound differentiate intrahepatic cholangiocarcinoma from hepatocellular carcinoma? *World J Gastroenterol*. 2020;26(27):3938-3951. [\[CrossRef\]](#)
18. Langenbach MC, Vogl TJ, von den Driesch I, et al. Analysis of Lipiodol uptake in angiography and computed tomography for the diagnosis of malignant versus benign hepatocellular nodules in cirrhotic liver. *Eur Radiol*. 2019;29(12):6539-6549. [\[CrossRef\]](#)
19. Hu XX, Wang WT, Yang L, et al. MR features based on LI-RADS identify cytokeratin 19 status of hepatocellular carcinomas. *Eur J Radiol*. 2019;113:7-14. [\[CrossRef\]](#)
20. Huang H, Tohme S, Al-Khafaji AB, et al. Damage-associated molecular pattern-activated neutrophil extracellular trap exacerbates sterile inflammatory liver injury. *Hepatology*. 2015;62(2):600-614. [\[CrossRef\]](#)
21. Llovet JM, Castet F, Heikenwalder M, et al. Immunotherapies for hepatocellular carcinoma. *Nat Rev Clin Oncol*. 2022;19(3):151-172. [\[CrossRef\]](#)
22. Chen Q, Wang M, Wang M, Jin S, Xiao SY, Tian S. Expansile invasive growth pattern is definite evidence for the diagnosis of small hepatocellular carcinomas: a comparative study of 37 cases. *Hum Pathol*. 2018;80:130-137. [\[CrossRef\]](#)
23. Chung YE, Kim MJ, Park YN, et al. Varying appearances of cholangiocarcinoma: radiologic-pathologic correlation. *Radiographics*. 2009;29(3):683-700. [\[CrossRef\]](#)
24. Zhang H, Yang T, Wu M, Shen F. Intrahepatic cholangiocarcinoma: epidemiology, risk factors, diagnosis and surgical management. *Cancer Lett*. 2016;379(2):198-205. [\[CrossRef\]](#)
25. Wang W, Gu D, Wei J, et al. A radiomics-based biomarker for cytokeratin 19 status of hepatocellular carcinoma with gadoxetic acid-enhanced MRI. *Eur Radiol*. 2020;30(5):3004-3014. [\[CrossRef\]](#)
26. Murakami Y, Kubo S, Tamori A, et al. Comprehensive analysis of transcriptome and metabolome analysis in intrahepatic cholangiocarcinoma and hepatocellular carcinoma. *Sci Rep*. 2015;5(1):16294. [\[CrossRef\]](#)
27. Panick CEP, Ward RD, Coppa C, Liu PS. Hepatic capsular retraction: an updated MR imaging review. *Eur J Radiol*. 2019;113:15-23. [\[CrossRef\]](#)
28. Park HJ, Kim YK, Cha DI, et al. Targetoid hepatic observations on gadoxetic acid-enhanced MRI using LI-RADS version 2018: emphasis on hepatocellular carcinomas assigned to the LR-M category. *Clin Radiol*. 2020;75(6):478. [\[CrossRef\]](#)
29. Shinmura R, Matsui O, Kobayashi S, et al. Cirrhotic nodules: association between MR imaging signal intensity and intranodular blood supply. *Radiology*. 2005;237(2):512-519. [\[CrossRef\]](#)
30. Alba AC, Agoritsas T, Walsh M, et al. Discrimination and calibration of clinical prediction models: users' guides to the medical literature. *JAMA*. 2017;318(14):1377-1384. [\[CrossRef\]](#)
31. Vittinghoff E, McCulloch CE. Relaxing the rule of ten events per variable in logistic and cox regression. *Am J Epidemiol*. 2007;165(6):710-718. [\[CrossRef\]](#)

Supplementary Table 1. Scanner sequences and parameter of MRI system									
Ingenia 3.0T					750W 1.5T				
Parameter	TSET2WI	DWI	3D-THRIVE	T1WI-mDIXON	FSET2WI	DWI	3D-LAVA	T1WI (in/out of phase)	
TR (ms)	2725	1353	3.7	3.7	8000	12857	5.04	5.4	
TE (ms)	78	72	1.32	1.32	82	66	2.31	2.3/1.2	
NEX	1	1	1	1	1	1	1	1	
Matrix	165 × 320	128 × 80	200 × 352	180 × 320	207 × 384	112 × 128	250 × 512	144 × 256	
FOV (mm ²)	285 × 214–285 × 380	285 × 214–285 × 380	285 × 214–285 × 380	285 × 214–285 × 380	330 × 330–380 × 380	330 × 330–380 × 380	330 × 330–380 × 380	330 × 330–380 × 380	
Inversion angle	140°	/	9°	70°	150°	/	10°	70°	
Slice thickness (mm)	5	5	4	4	7	7	4-5	7	
Slice gap (mm)	1	1	-2	-2	2.1	2.1	0	2.1	

TSE, turbo spin echo; T2WI, T2-weighted imaging; DWI, diffusion-weighted imaging; 3D-THRIVE, three dimension T1 high resolution isotropic volume examination; T1WI-mDIXON, T1-weighted imaging-modified DIXON; FSE, fast spin echo; 3D-LAVA, three dimension liver acquisition with volume acceleration; TR, repetition time; TE, echo time; NEX, number of excitation; FOV, field of view; MRI, magnetic resonance imaging.